E JOURNAL

Enhancing Dimensional Accuracy in Laser Powder Bed Fusion by Scaling Factor Optimization and 3D Scanner Capability Analysis

Stefan Brenner[1] · Vesna Nedeljkovic-Groha[1]

https://doi.org/10.58134/fh-aachen-rte_2024_009

[1]University of the Bundeswehr Munich, Institute for Design and Production Engineering, Werner-Heisenberg-Weg 39, 85579 Neubiberg, Germany

Abstract

In the laser-based powder bed fusion of metals (PBF-LB/M) process, part shrinkage occurs as a result of the repeated melting and solidification of metal powder and solid material during manufacturing, leading to thermally induced distortions. To improve the accuracy of the parts, the dimensional deviations are compensated for by using scaling factors, finite element simulations, or data-driven methods based on measurements. PBF-LB/M users often rely on optical measurement systems, such as 3D scanners, to measure the complex structures that are common in additive manufacturing. However, uncertainties in the 3D scan data and local surface errors are reasons for a lack of reliability in the dimensional accuracy assessment. In this study, we measure the positional accuracy and step heights of appropriately designed pin specimens, considering the tolerance fields of a structured light 3D scanner that comply with the required capability indices of measurement system analyses. Surface roughness measurements determine the tolerance fields for the diameter and roundness of the pins. By adjusting the scaling factors, we achieve a 70 % reduction in reproducible, systematic positional deviations, bringing them below the capability threshold of the 3D scanner. The diameter deviations and roundness are also smaller than the tolerance fields. Some of the step height errors are outside the tolerance but are one order of magnitude smaller than the local errors. The results of this study show the potential for improving dimensional accuracy through scaling factor optimization. For users of 3D scanners, it is important to consider the measurement capabilities when evaluating dimensional accuracy to verify the required tolerances.

Keywords Laser Powder Bed Fusion · Dimensional Accuracy · Scaling Factors · 3D Scanner · Capability Analysis

1. Introduction

In recent years, there has been significant progress in the development of Additive Manufacturing (AM) technologies for fabricating functional products. Laser-based powder bed fusion of metals (PBF-LB/M) has gained popularity as it enables the production of complex, lightweight, and customized parts with mechanical properties close to those of conventionally machined counterparts. PBF-LB/M achieves this by consolidating successive layers of powder through melting with a laser without the need for tools [1–4]. The inherent high level of complexity and the dynamics of the PBF-LB/M physical process contribute to the occurrence of defects in components, impeding its broader industrial use [1, 3]. Dimensional deviation is a basic problem in PBF-LB/M, which is due to thermal stresses that arise during the layer-by-layer build-up. Two descriptive models, the temperature gradient model (TGM) and the cool-down phase model, have been proposed in the literature to explain the evolution of thermal stresses in the PBF-LB/M process [2]. These models state that the recurring heating and cooling leads to thermal expansion and contraction, which is partly inhibited by surrounding material and leads to tensile stresses in the added top layers [2]. Large thermal stresses exceeding the yield strength will result in plastic deformation during the manufacturing process [5]. Thermally induced distortions and local errors, such as adhering powder particles or elevated part edges, are challenges in maintaining tight dimensional tolerances. Thermal material shrinkage is considered the main cause of insufficient dimensional accuracy [6, 7]. To broaden the industrial acceptance of AM parts and to improve the accuracy, dimensional deviations are compensated for by using scaling factors [8–12], finite element simulations [13–16], analytical models [17, 18], or data-driven methods based on measurements [6, 13, 19]. Due to the high engineering and computational effort of numerical AM analysis or the need for an initial part for measurement and derivation of data-driven compensation [6], a straightforward approach is to

perform shrinkage compensation by multiplying part dimensions by directional factors and measuring benchmark geometries for experimental validation.
Dao et al. [9] optimized the Shrinkage Compensation Factors (SCF) to reduce dimensional deviation caused by shrinkage of ABS plastic printed with Fused Deposition Modeling and used a digital caliper for measurements. Huang et al. [17] developed an analytical model to predict shrinkage in stereolithography, using SI500 resin, and measured cylinder shapes with a camera-based measuring system. Hartmann et al. [6] kept x, y, and z scaling factors constant and used 3D scan data for compensation of a fin-like part made from polyamide 12 using selective laser sintering. Raghunath & Pandey [11] optimized the scaling factors for the same process measuring cuboid samples with a screw gauge. Fotovvati & Asadi [8] kept x and y scaling factors (1.00236 and 1.00376 for Ti-6Al-4V) and beam offset in PBF-LB/M constant. A digital microscope was used for measurements. Zhang et al. [18] used a digital micrometer to validate their analytical model for calculating solidification shrinkage on thin-walled Ti-6Al-4V samples from PBF-LB/M. Yasa et al. [10] kept the x and y scaling factors constant (1.0021 and 1.0016 for AlSi10Mg) and optimized the z scaling factor for a thin-walled benchmark geometry. A coordinate measurement machine was used for measurements.
To better understand the position dependence, the distribution of simple samples over the entire substrate plate to indirectly assess the manufacturing precision of PBF-LB/M systems is proposed [20]. Calipers [21], coordinate measuring machines [22] and screw gauges [23] are used to measure cube or cylinder samples to determine position-dependent accuracy. It is a challenge to use tactile systems to measure complex structures [24], such as those frequently found in AM, and to assess whether they meet the tolerance requirements. The dimensional accuracy of functional parts or prototypes [15, 16, 19, 25, 26] or benchmark artifacts [1, 8, 11, 27–33] is therefore often assessed using structured light 3D scanners. These optical systems are usually available in AM facilities [31] and are reported to be particularly useful for high-precision measurement of smaller PBF-LB/M geometries [27].
However, the limitations of 3D scan measurements, concerning the measuring equipment capability, have not yet been discussed in depth in this context. The literature shows measurement uncertainties of 4 µm to 25 µm for structured light 3D scanners [1, 24, 33, 34]. Vagovský et al. [35] state that a structured light 3D scanner type commonly used for PBF-LB/M geometries did not meet the requirements of a measurement system analysis. It is not considered capable of measuring small objects with tight tolerances, e.g. a ø12h6 cylinder (tolerance field: 11 µm) coated with matting spray. Depending on the measuring volume and the evaluation method, it was not even capable of measuring ø12h9 (tolerance field: 43 µm). They state that the 3D scanner is not primarily intended for scanning and measuring such small and precise objects. This opens the question about the reliability of measurements from structured light 3D scanners in the context of PBF-LB/M examination.
In this study, we determine the measurement capability of a structured light 3D scanner and use it as tolerance limits for accuracy optimization in PBF-LB/M. We inform users of PBF-LB/M and 3D scanners about the accuracy that can be reliably measured and define scaling factors and a beam compensation value that improve the overall accuracy.

2. Material and methods

2.1. Metal powder and PBF-LB/M system

The AlSi10Mg powder material used in this work (nominal particle size distribution: 20 µm to 63 µm) is purchased from SLM Solutions (Lübeck, Germany) and is used in recycled condition. An SLM125^{HL} PBF-LB/M system from SLM Solutions with a build envelope of 125×125×125 mm³ was used to manufacture the specimens. The main process parameters are listed in Table 1. The Shrinkage Compensation Factors (SCF) and the Beam Compensation (BC) shown are the default values and may be adjusted as required (see Chapter 2.3).

Table 1: PBF-LB/M main process parameters for AlSi10Mg.

Parameter	Volume	Contour
Power (W)	350	300
Scan speed (mm/s)	1650	730
Hatch distance (mm)	0.13	-
BC (mm)	-	0.17*
SCF_{xy} (-)	1.0033*	
SCF_{z} (-)	1.0000*	

*Adjustable in this study

A layer thickness of 30 µm and a rotating stripe scan strategy were used. The platform was preheated to 150°C and the build chamber was inerted with argon.

2.2. Pin specimen design and arrangement

We aim to use simple specimens distributed over the entire substrate plate as suggested by Giorgetti et al. [20]. The specimens were appropriately designed as cylindrical pins with two truncated cones at the upper

ends (hereinafter: pins) to fulfill several purposes. Firstly, the pins are big enough to print smoothly with standard parameters. Secondly, they are small enough to place a sufficient number of them on the SLM125^{HL}'s substrate plate while leaving enough space between them so that they do not obscure each other during 3D scanning. Thirdly, they contain simple but meaningful geometrical features such as cylinders and parallel planes, from which information about position, diameter, roundness, and step height can be derived. The dimensions of the pins are shown in Figure 1a) and the arrangement pattern in Figure 1b). The pins are printed on 2 mm high supports (not shown in the drawing) so that the upper plane is at a build height of 12 mm. With 13.5 mm even spacing in the x and y directions, 65 pins fit on the substrate plate, leaving the corners free because of the screw holes (red symbols).

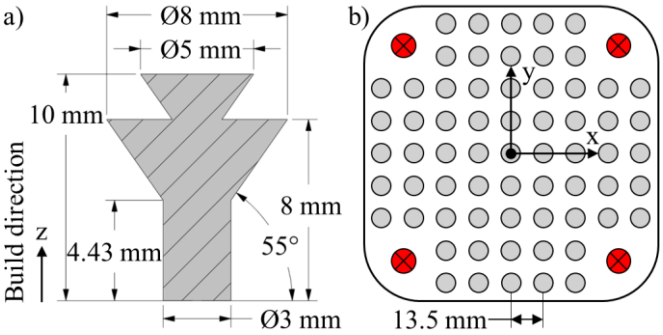

Figure 1: a) Pin specimen dimensions in sectional drawing. b) Arrangement pattern of 65 pins on the substrate plate.

Cylindrical substrate plates are also common in PBF-LB/M systems. In this case, a pattern of evenly spaced pins in concentric circles with radii of 13.5 mm steps would be preferable and describing the positions of the pins in a cylindrical coordinate system would be advantageous.

2.3. Scaling and compensation methods

Materialise Magics 23.0 software with the SLM Build Processor 3.0.216.0 was used for the digital pre-processing. After importing the CAD model of the pin and creating the pattern, several options are available to adjust the parts before manufacturing. We focus on the possibilities to account for shrinkage compensation and positioning adjustment. Magics offers scaling options in the CAD preparation stage and the later slicing stage. In the CAD preparation stage, scaling operations are possible for each part individually. The scaling factors used there are referred to here as Individual Part Scaling Factors (IPSF). In the slicing stage, the scaling operations apply equally to all parts and are intended to compensate for material-dependent shrinkage. These scaling factors are referred to here as shrinkage compensation factors (SCF). For all scaling factors, the directional components can be changed independently in the x, y, and z directions. For both IPSF and SCF, the part center or the origin of the coordinate system can be defined as the scaling center. Figure 2 shows these two methods schematically with a scaling factor > 1. Regardless of whether IPSF or SCF is used, parts on the substrate plate can be scaled 1) around their center point, resulting in dimensional changes while the center point of the part remains in place, or 2) from the origin, resulting in dimensional changes and a positional shift.

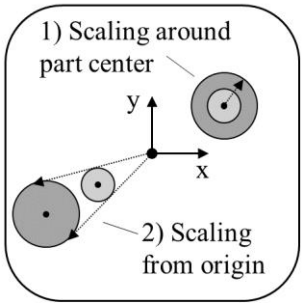

Figure 2: Scaling of a small circle (light gray) with a scaling factor > 1. Scaling around the part center (1) leads to dimensional changes only. Scaling from the origin (2) leads to dimensional changes and a position shift.

It is worth noting that regardless of whether method 1) or 2) is selected for the SCF, only the effect of method 1) comes into play. When inspecting the build files, no shift in position can be seen for method 2). Since this behavior cannot currently be explained, we only selected either IPSF or SCF not equal to 1 to avoid unwanted interactions.
Within the SLM Build Processor, the BC can be defined as well. This factor, also referred to as beam offset in the literature, takes into account the melt pool width and offsets the CAD model contour inwards [36, 37].

2.4. Tolerance limits for 3D scanner measurements

A VL-550 structured light 3D scanner from Keyence (Osaka, Japan) with a specified measurement accuracy of ± 10 µm and repeatability of 2 µm is used for optical measurements. The tolerance limits for the positioning and the step height of the pins come from Measurement System Analyses (MSA) conducted with the Structured Light 3D Scanner (SLS). Following the industrially established method of Robert Bosch GmbH [38] with 50 repeated measurements of a known reference, the potential capability indices C_g and the critical capability indices C_{gk} are calculated according to

$$C_g = \frac{0.2 \times T}{6 \times s} \quad (1)$$

$$C_{gk} = \frac{0.1 \times T - |\bar{x} - x_{Ref}|}{3 \times s} \quad (2)$$

with the mean value $\bar{x}$, the standard deviation s and the reference value x_{Ref}. The difference between $\bar{x}$ and x_{Ref} is also referred to as bias. The tolerance field T is increased until the capability criteria $C_g \geq 1.33$ and $C_{gk} \geq 1.33$ are just met. This proves that the SLS is capable of measuring distances and step heights, taking into account the central tendency and variability within the respective tolerance field. We use a ceramic ball gauge and a ceramic step gauge purchased from Keyence with certificated reference values x_{Ref} for nominal ball distances of 40 mm and 120 mm and a nominal step height of 2 mm. The settings for the composition of 16 individual scans (4 pivot points and 4 viewing angles) to a 360° total result per measurement run are retained for the subsequent examination of the AlSi10Mg specimens. Without post-processing steps, the surface roughness of PBF-LB/M parts is a limiting factor for dimensional accuracy. To determine tolerance limits for the diameter and roundness of the pins, the surface roughness is examined using a Keyence VR-5000 wide-area 3D profilometer. This device resolves surfaces much finer (approx. 17.300 triangles per mm² on an exported STL file) than the SLS (approx. 1.600 triangles per mm²) does and can capture adhering powder particles or elevated part edges in detail. These local errors create roughness on the surfaces which compromises the shape of the pins. An area of 2×3 mm² was measured on the cylindrical part of several pins with 40× magnification in high-resolution mode. Processing steps according to ISO 25178-2:2012 with a cylinder shape correction, a high-pass filter (L-filter) of 0.8 mm, and an end effect correction were applied in the Keyence software. The maximum height Sz is evaluated as a measure of tolerance limits for the diameter and roundness. The tolerance limits determined in this way serve as range limits within which the 3D scanner cannot provide reliable information about the scattering behavior of the measured values.

As can be seen from equations (1) and (2), any measurement system can fulfill the capability criteria by increasing the tolerance field T. A large T encompasses the measured values and pretends that the reliably measurable optimization potential has been exhausted. Therefore, the use of adequate, certified, and maintained measurement systems by trained personnel is a prerequisite. To enhance the generalizability of our findings to other 3D scanners, we generated additional tolerance values meeting the capability criterion $C_{gk} = 1.33$ based on synthetic data. To achieve this, normally distributed random numbers at two levels each for the bias and the standard deviation were generated numerically. This approach simulates measurement data comparable to that obtained from any 3D scanner with a similar accuracy as the device used in this study. 100 sets of 50 synthetic values (for 50 repeated measurements according to Robert Bosch GmbH [38]) were generated for the four factor combinations to ensure the robustness and reliability of the results. From this, we derived a best-fit regression equation that relates the predicted tolerance field $T_{predicted}$ to the accuracy parameters bias and standard deviation s in the form of

$$T_{predicted} = b_0 + b_1 \times \text{bias} + b_2 \times s \quad (3)$$

with the coefficients b_0, b_1 and b_2.

The substrate plate and the pins on it (hereinafter: build job) are coated with a thin layer of the scanning spray induscan`spray from Dentaco (Essen, Germany) before the measurements to avoid light reflections. The coating is applied manually using a spray can. Coating is a standard preparation of scanned objects to enable proper measurements. According to the spray supplier, the coating thickness is less than 5 µm. This is smaller [39] or similar [40] to coating thicknesses reported in the literature for comparable sprays. Therefore, the coating thickness applied to the pins is likely to be significantly lower than the expected roughness $Rz \leq 72$ µm [41] and is not examined in more detail.

2.5. Measurement procedure and evaluation

The build jobs are 360° scanned with the SLS. The coordinate system of the 3D scan needs to be aligned with the PBF-LB/M system. For this, the side planes of the substrate plate are extracted from scanned build jobs. In case of a cuboid substrate plate, there are four planes X_-, X_+, Y_-, and Y_+(see schematic in Figure 3). The median planes X_m and Y_m are derived from the opposing planes. From the top surface of the substrate plate on which the pins are built, the plane Z_0 is extracted. The intersection of the planes X_m, Y_m, and Z_0 forms the coordinate origin. The x-y plane lies in Z_0 and the x-axis follows the normal vector of X_m.

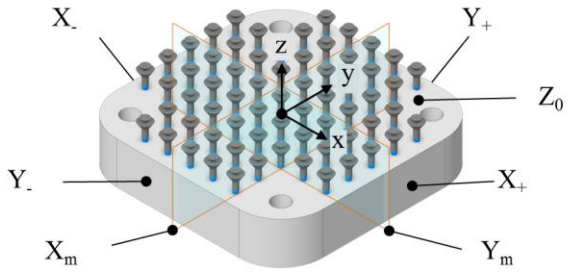

Figure 3: Coordinate system in the 3D scan (schematic).

In case of a cylindrical substrate plate, the coordinate origin is determined as the intersection of the cylinder axis and the Z_0 plane. The positions of the pins are determined by their cylinder centers. For this purpose,

three planes Z_3, Z_4, and Z_5 are created parallel to Z_0 at build heights z = 3 mm, 4 mm and 5 mm to generate profile sections in the scan data (Figure 4).

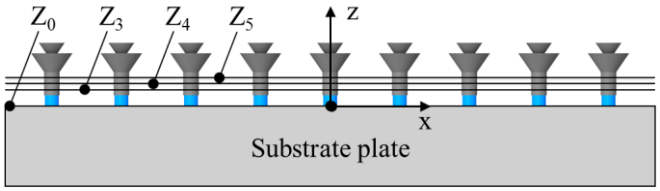

Figure 4: Planes for cross-section profiles at heights 3 mm, 4 mm, and 5 mm. Supports at build height 0 mm < z < 2 mm for connecting the pins to the substrate plate are shown in blue.

A best-fit circle is inserted into the cross-section of each pin, and the mean value of the x and y coordinates of its center point from the three Z planes describes the measured positions in x direction (x_M) and in y direction (y_M) of a pin. The SLM125^{HL}'s substrate plate is fixed to the build platform using screws during machine setup. Its position is not defined by stops or dowel pins, resulting in an undefined x-y plane position within the clearance between the screws and the holes. This potential cause of pin positional deviations is omitted in this study, considering that other additive manufacturing systems have substrate plate centering and this aspect is therefore not of interest to all users. Consequently, a position correction is implemented to align the central pin with the coordinate origin. The position deviation f_{PS} and the position tolerance t_{PS} are then calculated according to Klein [42] using the equation

$$f_{PS} = \sqrt{(x_M - x_{theo})^2 + (y_M - y_{theo})^2} \leq \frac{t_{PS}}{2} \quad (4)$$

$$f_{PS} = \sqrt{(\Delta x)^2 + (\Delta y)^2} \leq \frac{t_{PS}}{2}$$

with the ideal position components x_{theo} and y_{theo}. The differences between the measured position and the ideal position in x and y directions are referred to as Δx and Δy, respectively. The mean values of the diameter D_M and the roundness R are also determined using the best-fit circles for each pin in the Keyence software. We use roundness as a measure of form deviation, i.e. the radial distance between two concentric circles, one maximum inscribing, the other minimum circumscribing the measured cross-section of a pin [43].

To determine the step height, planes are fitted in the surfaces of the lower and upper cones. The visibly elevated edges are excluded from the fitting operation. The measured step height z_M is the z-distance between these two planes using the parallel restraint in the Keyence software. The deviations of the diameter ΔD and the step height Δz are calculated by subtracting the nominal values from the measured values according to $\Delta D = D_M - 3$ mm and $\Delta z = z_M - 2$ mm.

3. Results and discussion

3.1. Tolerance limits from measurement system analyses and surface roughness

During the measurement system analyses (MSA), the distances between ball centers and the step height in ceramic gauges were measured and evaluated using the SLS. The measurement results and capability indices are shown in Table 2.

Table 2: Results of measurement system analyses for VL-550 SLS. The values of the tolerance field T are adjusted to reach $C_g \geq C_{gk} \geq 1.33$. $T_{predicted}$ is calculated by inserting the measured biases and standard deviations into equation (3) from the regression model.

Gauge	Ball		Step
Nominal value (mm)	40	120	2
x_{Ref} (mm)	40.0018	120.0090	1.9989
$\bar{x}$ (mm)	40.0025	120.0179	1.9989
s (mm)	0.0027	0.0073	0.0005
T (mm)	0.1148	0.3801	0.0223
$T/2$ (mm)	0.0574	0.1901	0.0112
$T_{predicted}$ (mm)	0.1192	0.3760	0.0252
C_g (-)	1.41	1.74	1.36
C_{gk} (-)	1.33	1.33	1.33

The mean values of the measured, horizontal ball distances are slightly larger than the certificate values, but are within the specified measurement accuracy of ± 10 µm. The vertical step height was exactly measured. The following statements summarize the results of the MSA and describe the capability of the SLS:

- At a horizontal distance of 40 mm, a measurement error of 0.7 µm with a standard deviation of 2.7 µm results in a tolerance field of 114.8 µm.
- At a horizontal distance of 120 mm, a measurement error of 8.9 µm with a standard deviation of 7.3 µm results in a tolerance field of 380.1 µm.
- At a vertical step height of 2 mm, a measurement error of 0.0 µm with a standard deviation of 0.5 µm results in a tolerance field of 22.3 µm.

$\pm \frac{T}{2}$ will span the tolerance field around the nominal distances. The MSA shows that the SLS is capable of measuring a nominal distance of 40 mm with ± 0.0574 mm. Accordingly, it can measure the distance

120 mm ± 0.1901 mm and the step height 2 mm ± 0.0112 mm. For distances between 40 mm and 120 mm, linear interpolation is used to estimate the tolerance field. It is worth noting that the MSA reveals far greater tolerances for the SLS than the measurement accuracy specified in the data sheet (± 10 µm). In order to gain a better understanding of achievable tolerances with structured light 3D scanners, synthetic data was also evaluated (see Chapter 2.4). The mean tolerance values derived from 100 sets of 50 random numbers were utilized as input for a multiple linear regression analysis, resulting in the coefficients $b_0 = 0.00526$, $b_1 = 8.96$, and $b_2 = 39.869$. The regression model exhibited significance with a p-value of 0.025 and an adjusted R-Square of 0.998. Notably, the predicted tolerances closely aligned with the measured tolerances in Table 2. In scenarios that correspond to the data sheet specifications of the measurement system, i.e. the standard deviation equals the repeatability of 2 µm and the bias is based on the accuracy between 0 µm and 10 µm, the model delivers $T_{predicted}$ between 0.0850 mm and 0.1746 mm. In these scenarios, the tolerances significantly exceed the accuracy specification. The regression model offers a way to estimate the capabilities of 3D scanners based on data sheet specifications without the need for expensive, high-precision reference gauges. Even with a well calibrated and adjusted device, the model coefficient b_2 shows a multiple of about 40 of the repeatability to obtain a good first estimate of the tolerance zone that meets the capability requirements.

The 3D profilometer measurement shows a surface roughness of Sz = 91.5 µm ± 3.9 µm on the pins coated with scanning spray. This roughness corresponds to the specifications in the VDI material data sheet for AlSi10Mg (Rz from 72 µm to 141 µm) [41]. Figure 5 shows a height profile on the unwrapping of the lateral surface of a pin's cylindrical part. The non-periodic height profile shows local peaks and valleys approx. between -0.05 mm and 0.05 mm according to the measured roughness values. The supports were not included in the roughness measurements.

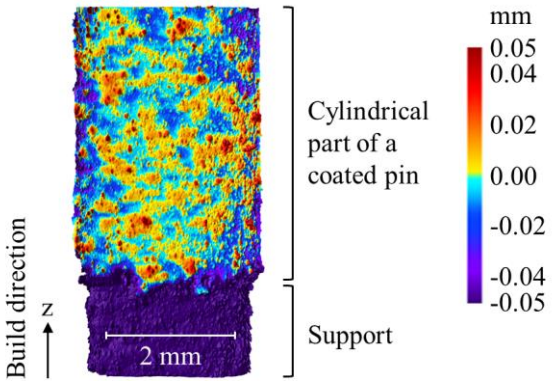

Figure 5: Non-periodic height profile on the unwrapping of the lateral surface of a coated pin (3D profilometer image).

Tolerance limits of $\pm \frac{Sz}{2} = \pm$ 0.0458 mm are used for the diameter and roundness measurements.

3.2. Position

The positional accuracy of the pins arranged in the 13.5 mm spaced pattern is evaluated using the positional deviation in the x and y directions as a function of the position of the respective pin on the substrate plate. Position deviations $f_{PS} \leq 0.190$ mm are present in build job 1 printed with standard parameters (mean value ± standard deviation: $\overline{f_{PS}} = 0.118$ mm ± 0.044 mm). In Figure 6 and Figure 7, the deviation components Δx and Δy are shown depending on the x and the y position, respectively. The red lines indicate the tolerance field with $\pm \frac{T}{2}$ from the ideal position. The slopes for x < -40 mm and x > 40 mm result from the linear interpolation to the next known tolerance field value at x = ± 120 mm. Taking these tolerances into account, the SLS can only reliably measure the deviations that lie outside the tolerance field limits. It is evident that Δx only depends on x and Δy only depends on y.

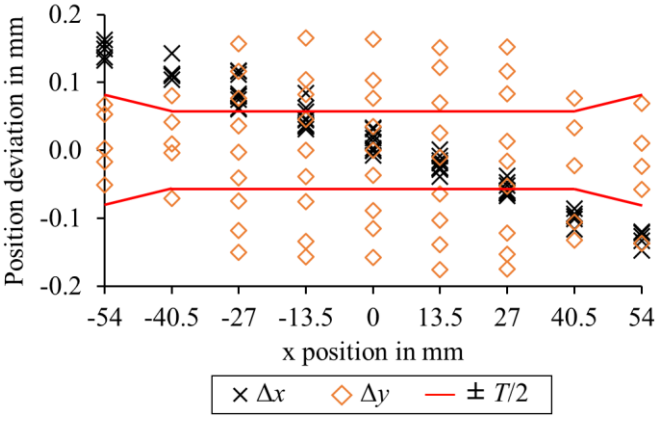

Figure 6: Position deviations of the pins depending on the x position. Build job 1 with standard parameters.

Δx correlates strongly negatively with the x position, where positive Δx are found at negative x positions. This means, for example, that the pins on the left edge of the substrate plate (x = -54 mm) are about 0.15 mm too far to the right ($\Delta x \approx 0.15$ mm) and therefore too close to the center. The same applies to the right edge (x = 54 mm), where the pins are positioned too far to the left ($\Delta x \approx$ -0.15 mm) and therefore also too close to the center. Δy strongly scatters along the x position without correlation. Along the y position (Figure 7), Δx and Δy behave the opposite way. This deviation behavior could be reproduced in a repeated build job with standard parameters (build job 2) but with a little lower position deviations $f_{PS} \leq 0.176$ mm (mean value ± standard deviation: $\overline{f_{PS}} = 0.100$ mm ± 0.040 mm).
The position deviations determined in this study are smaller than the values of 0.3 mm found by Gruber et al. [28] for 2 mm cylinder samples. They used an artifact containing printed cylinders and datum planes. Therefore, the samples were not examined directly on the substrate plate, which may lead to higher position deviations.

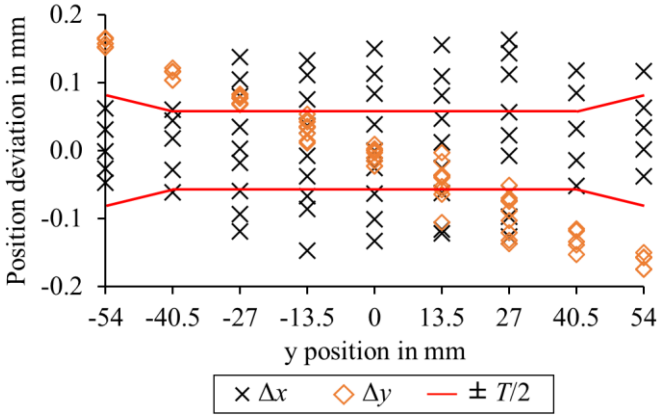

Figure 7: Position deviations of the pins depending on the y position. Build job 1 with standard parameters.

Because many measured values are outside the tolerance range, there is potential for minimizing the deviations that can be reliably detected by the 3D scanner. Since the position dependence of the deviations is recognized, we aim to increase the shift of the pin positions away from the center.
In the following, the scaling factors are varied using the scaling from the origin method for IPSF (see Chapter 2.3) to minimize the position deviations f_{PS} and the position tolerances t_{PS}, respectively. Table 3 provides an overview of the combinations of scaling factors used in the pre-process of the build jobs, including the color assignment used in the following charts.

Table 3: Scaling factor combinations used in build jobs 1 - 5.

Build job	Color assignment	$IPSF_{xy}$ (-)	SCF_{xy} (-)	BC (mm)
1 & 2	Black*	1	1.0033	0.170
3	Gray	1.0053	1	0.170
4	Cyan	1.0022	1	0.120
5	Green	1.0027	1	0.155

*Standard parameters. $IPSF_z = SCF_z = 1$.

The results of the parameter variations are shown in Figure 8, where the position tolerance t_{PS} is plotted over the distance from the center $d = \sqrt{{x_{theo}}^2 + {y_{theo}}^2}$. For build job 1 with standard parameters (black), it can be seen that $t_{PS} = 2 \times f_{PS}$ increases with increasing d. The same is true for build job 3 (gray), where SCF_{xy} was set to 1, $IPSF_{xy}$ was increased and BC kept constant. t_{PS} is equally large and the mean position deviation $\overline{f_{PS}} = 0.123$ mm ± 0.045 mm is also similar to build jobs with standard parameters, but the deviations are due to an excessive shift in position. The pins are too far from the center and the correlations of Δx and Δy with the x and y position change sign compared to the standard parameters. At a distance from the center $d > 20$ mm, t_{PS} is above the tolerance limit and can therefore be reliably determined.

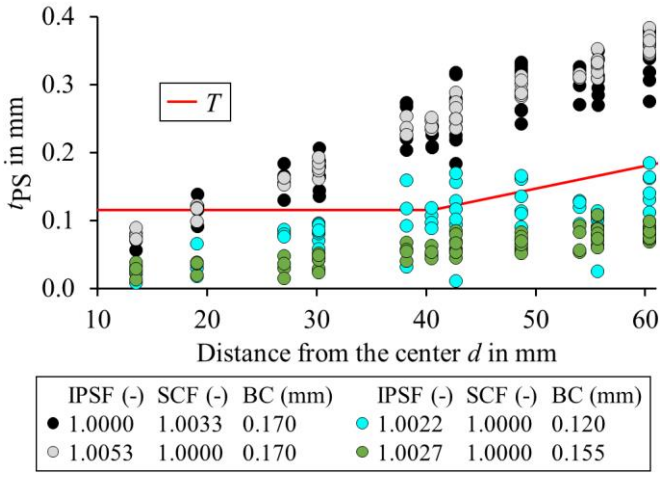

Figure 8: Position tolerance t_{PS} along the distance from the center d for build jobs with four parameter combinations.

$IPSF_{xy}$ is reduced in build job 4 (cyan). Since with $1 < IPSF_{xy} < 1.0033$ and $SCF_{xy} < 1.0033$, the overall scaling in x-y is smaller than with standard parameters and the enlargement of the geometry may not be sufficient to compensate for the shrinkage, BC is reduced to account for this effect. Much better positional accuracy was achieved ($\overline{f_{PS}} = 0.047$ mm ± 0.022 mm), but some pins still show potential for improvement with

$t_{PS} > T$. Next, $IPSF_{xy}$ and BC are slightly increased again in build job 5 (green) what leads to further improvement of $\overline{f_{PS}} = 0.029$ mm ± 0.012 mm and no more $t_{PS} > T$ is found. As all measured values fall below the capability of the measurement system, the potential for verifiable position optimization is exhausted. In the following, we focus on this most promising parameter combination with $IPSF_{xy} = 1.0027$, $SCF_{xy} = 1$, and BC = 0.155 mm (hereinafter: optimized parameters). $IPSF_{xy}$ is close to the x and y scaling parameters for AlSi10Mg of Yasa et al. [10], for which they confirm sufficient dimensional accuracy.

3.3. Diameter and roundness

The scaling method used to improve the positional accuracy of the pins also changes the part geometry in the x-y plane as described in Chapter 2.3. The effects on dimensional accuracy are investigated based on the diameter and roundness of the pins. The diameter deviations ΔD along the distance from the center d are shown in Figure 9. With standard parameters (black), ΔD scatters wide within the tolerance limits from the surface roughness and only a few values are outside. The optimized parameters (green) show a tighter scattering of ΔD with a slightly negative mean value $\overline{\Delta D} = -0.023$ mm, but no values outside the tolerance limits. There is no clear correlation between ΔD and d. The potential for improving dimensional accuracy is limited, as the diameter deviations are superimposed by the roughness.

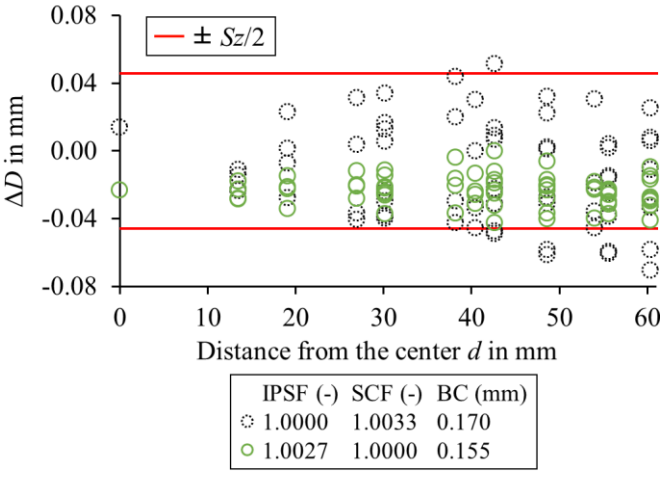

Figure 9: Deviations of the diameter ΔD along the distance from the center d for build jobs with standard (black) and optimized (green) parameters.

$IPSF_{xy}$ could be slightly increased, which could also be favorable for the position deviation. Gradl et al. [1] reported a negative diameter deviation of -0.013 mm (read from figure) for 3 mm pins and Gruber et al. [28] found approx. 5 % relative deviation (read from figure) for 2 mm pins, which equals 0.1 mm. Regarding the roundness R, most of the values from standard parameters (black), are above the roughness (Figure 10).

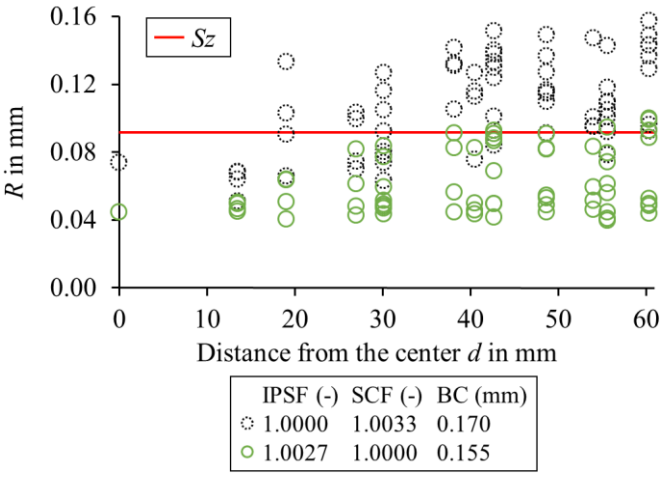

Figure 10: Roundness R along the distance from the center d for build jobs with standard (black) and optimized (green) parameters.

The roundness R correlates positively with the distance from the center d but with a weak coefficient of determination of 0.3. Morvayova et al. [22] also found increasing distortions of AlSi10Mg cube specimens towards the edges of the build plate. They attribute the influence of the position on the dimensional accuracy to the difference in the thermal fields on the substrate plate. The values from optimized parameters (green) are almost entirely lower than the roughness and show an even weaker positive correlation with d (coefficient of determination: 0.08). Veetil et al. [23] found a systematic, elliptical deformation of the 10 mm stainless steel 316L cylinders, which they attributed to the shielding gas flow. Such an effect could be reduced by choosing $IPSF_x \neq IPSF_y$ to compensate for asymmetrical deviation, but the pins in this study show no systematic form deviation. The roundness is mainly affected by local defects on the surface. Interestingly, it improves despite the adjusted parameters do not directly influence the shape.

3.4. Step height

The z scaling factor remained equal to 1 so no effects are expected regarding the step height. Figure 11 shows the step height deviations Δz along the distance from the center d for standard (black) and optimized (green) parameters.

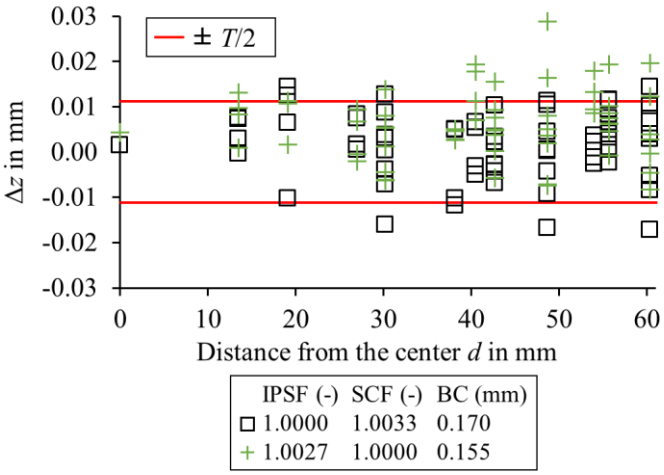

Figure 11: Deviations of the step height Δz along the distance from the center d for build jobs with standard (black) and optimized (green) parameters.

Only approx. 20 % of Δz values are outside the tolerance limit with no value below the lower limit for the optimized parameters. The mean deviation of the step height $\overline{\Delta z}$ is 0.006 mm, which suggests a slight downscaling of the pins. To put Δz into perspective, the y-axis of the chart spans 60 µm which is approx. the D90 value of the used AlSi10Mg powder. This means, that 10 % of the powder particles are bigger than the shown y-axis section. Moreover, the pins show elevated edges which are one order of magnitude bigger than Δz. The optimization potential of z scaling is low compared to measures for improving the elevated edges, e.g. by adjusting the contour process parameters. Morvayova et al. [22] measured z shrinkages of -0.10 mm to -0.46 mm for 35 mm AlSi10Mg cube specimens. In this case, z scaling would improve the dimensional accuracy.

4. Conclusion and outlook

In this study, we assessed the positional and dimensional accuracy of AlSi10Mg specimens produced using PBF-LB/M, employing a structured light 3D scanner. The arrangement of 65 appropriately designed pin specimens on the substrate plate enabled this evaluation. Measurement system analyses were carried out to determine the capability of the 3D scanner. Although all reference values could be measured within the measurement accuracy specification (± 10 µm), the tolerance fields must be significantly larger to meet the capability requirements for the measurement system analyses. The 3D scanner is capable of measuring horizontal distances of 40 mm and 120 mm with tolerance fields of 0.1148 mm and 0.3801 mm and a step height of 2 mm with a tolerance field of 0.0223 mm. Both the measurements and the coefficient b_2 from the multiple linear regression determined in this study indicate that approximately 40 times the repeatability of a 3D scanner serves as a suitable initial estimate for the tolerance range within which the device can measure to meet the requirements of a measurement system analysis. The tolerance fields and a surface roughness of Sz = 91.5 µm served as limits for scaling parameter and beam compensation optimization. Reproducible, systematic positional deviations were identified and improved by 70 % using an adjusted x-y scaling factor of 1.0027 and a beam compensation of 0.155 mm. Diameter and roundness were within the determined capability limits. The step heights of the pins show slight optimization potential for z scaling, but no z scaling was applied because the maximum height deviations are one order of magnitude smaller than local errors such as elevated part edges. Thermally induced shrinkage was successfully compensated for and the overall accuracy was improved. 3D scanner users benefit from quantitative information about measurement capabilities when assessing dimensional accuracy.
Possible future work may include larger specimens to assess the accuracy at greater build heights within the entire build envelope.

5. Acknowledgement

The equipment and material from the FLAB-3Dprint research project used in this study are funded by dtec.bw – Digitalization and Technology Research Center of the Bundeswehr which we gratefully acknowledge. dtec.bw is funded by the European Union – NextGenerationEU.

6. Contributions

Conceptualization, S. Brenner (S.B.) and V. Nedeljkovic-Groha (V.N.-G.); methodology, S.B.; software, S.B.; validation, S.B. and V.N.-G.; formal analysis, S.B.; investigation, S.B.; resources, V.N.-G.; data curation, S.B.; writing—original draft preparation, S.B. and V.N.-G.; writing—review and editing, S.B. and V.N.-G.; visualization, S.B.; supervision, V.N.-G.; project administration, S.B.; funding acquisition, V.N.-G. All authors have read and agreed to the published version of the manuscript.

References

[1] P. R. Gradl, D. C. Tinker, J. Ivester, S. W. Skinner, T. Teasley, and J. L. Bili, "Geometric feature reproducibility for laser powder bed fusion (L-PBF) additive manufacturing with Inconel 718," *Addit. Manuf.*, vol. 47, p. 102305, 2021, doi: 10.1016/j.addma.2021.102305.

[2] J.-P. Kruth, J. Deckers, E. Yasa, and R. Wauthlé, "Assessing and comparing influencing factors of residual stresses in selective laser melting using a novel analysis method," *Proc. Inst. Mech. Eng. Part B J. Eng. Manuf.*, vol. 226, no. 6, pp. 980–991, 2012, doi: 10.1177/0954405412437085.

[3] Y. Zhang, J. Y. Fuh, D. Ye, and G. S. Hong, "In-situ monitoring of laser-based PBF via off-axis vision and image processing approaches," *Addit. Manuf.*, vol. 25, pp. 263–274, 2019, doi: 10.1016/j.addma.2018.10.020.

[4] D. Xie, F. Lv, H. Liang, L. Shen, Z. Tian, J. Zhao, Y. Song, and C. Shuai, "Towards a comprehensive understanding of distortion in additive manufacturing based on assumption of constraining force," *Virtual Phys. Prototyp.*, vol. 16, sup1, S85-S97, 2021, doi: 10.1080/17452759.2021.1881873.

[5] J. L. Bartlett and X. Li, "An overview of residual stresses in metal powder bed fusion," *Addit. Manuf.*, vol. 27, pp. 131–149, 2019, doi: 10.1016/j.addma.2019.02.020.

[6] C. Hartmann, P. Lechner, B. Himmel, Y. Krieger, T. C. Lueth, and W. Volk, "Compensation for Geometrical Deviations in Additive Manufacturing," *Technologies*, vol. 7, no. 4, p. 83, 2019, doi: 10.3390/technologies7040083.

[7] F. Calignano, "Investigation of the accuracy and roughness in the laser powder bed fusion process," *Virtual Phys. Prototyp.*, vol. 13, no. 2, pp. 97–104, 2018, doi: 10.1080/17452759.2018.1426368.

[8] B. Fotovvati and E. Asadi, "Size effects on geometrical accuracy for additive manufacturing of Ti-6Al-4V ELI parts," *Int. J. Adv. Manuf. Technol.*, vol. 104, 5-8, pp. 2951–2959, 2019, doi: 10.1007/s00170-019-04184-1.

[9] Q. Dao, J. C. Frimodig, H. N. Le, X.-Z. Li, S. B. Putnam, K. Golda, J. Foyos, R. Noorani, and B. Fritz, "Calculation of shrinkage compensation factors for rapid prototyping (FDM 1650)," *Comput. Appl. Eng. Educ.*, vol. 7, no. 3, pp. 186–195, 1999, doi: 10.1002/(SICI)1099-0542(1999)7:3<186::AID-CAE7>3.0.CO;2-Q.

[10] E. Yasa, I. Kandemir, and I. Atik, "On the Z-dimensional accuracy of L-powder bed fusion," *J. Addit. Manuf. Technol.*, vol. 1, no. 2, p. 533, 2021, doi: 10.18416/JAMTECH.2111533.

[11] N. Raghunath and P. M. Pandey, "Improving accuracy through shrinkage modelling by using Taguchi method in selective laser sintering," *Int. J. Mach. Tools Manuf.*, vol. 47, no. 6, pp. 985–995, 2007, doi: 10.1016/j.ijmachtools.2006.07.001.

[12] Y. Liu, Y. Yang, and D. Wang, "Investigation into the shrinkage in Z-direction of components manufactured by selective laser melting (SLM)," *Int. J. Adv. Manuf. Technol.*, vol. 90, pp. 2913–2923, 2017, doi: 10.1007/s00170-016-9596-y.

[13] S. Afazov, W. A. Denmark, B. Lazaro Toralles, A. Holloway, and A. Yaghi, "Distortion prediction and compensation in selective laser melting," *Addit. Manuf.*, vol. 17, pp. 15–22, 2017, doi: 10.1016/j.addma.2017.07.005.

[14] T. Frigioescu, G. Matache, T. Badea, and D. Ionita, "Distortion compensation of IN 625 parts manufactured by selective laser melting," in vol. 2302, *AIP Conference Proceedings*: AIP Publishing, 2020, p. 120005. Accessed: Oct. 30 2022, doi: 10.1063/5.0033743.

[15] C. Seidel and M. F. Zaeh, "Multi-scale Modelling Approach for Contributing to Reduced Distortion in Parts Made by Laser-based Powder Bed Fusion," *Procedia CIRP*, vol. 67, pp. 197–202, 2018, doi: 10.1016/j.procir.2017.12.199.

[16] F. Zongo, C. Simoneau, A. Timercan, A. Tahan, and V. Brailovski, "Geometric deviations of laser powder bed–fused AlSi10Mg components: numerical predictions versus experimental measurements," *Int. J. Adv. Manuf. Technol.*, vol. 107, no. 3, pp. 1411–1436, 2020, doi: 10.1007/s00170-020-04987-7.

[17] Q. Huang, J. Zhang, A. Sabbaghi, and T. Dasgupta, "Optimal offline compensation of shape shrinkage for three-dimensional printing processes," *IIE Transactions*, vol. 47, no. 5, pp. 431–441, 2015, doi: 10.1080/0740817X.2014.955599.

[18] L. Zhang, S. Zhang, H. Zhu, Z. Hu, G. Wang, and X. Zeng, "Horizontal dimensional accuracy prediction of selective laser melting," *Mater. Des.*, vol. 160, pp. 9–20, 2018, doi: 10.1016/j.matdes.2018.08.059.

[19] M. McConaha and S. Anand, "Additive Manufacturing Distortion Compensation Based on Scan Data of Built Geometry," *J. Manuf. Sci. Eng.*, vol. 142, no. 6, p. 61001, 2020, doi: 10.1115/1.4046505.

[20] A. Giorgetti, F. Ceccanti, P. Citti, A. Ciappi, and G. Arcidiacono, "Axiomatic Design of Test Artifact for Laser Powder Bed Fusion Machine Capability Assessment," *MATEC Web Conf.*, vol. 301, p. 6, 2019, doi: 10.1051/matecconf/201930100006.

[21] M. Schmitt, G. Schlick, and J. Schilp, "Repeatability of Dimensional Accuracy and Mechanical Properties in Powder Bed Fusion of 16MnCr5 using a Laser Beam," *Procedia CIRP*, vol. 114, pp. 94–99, 2022, doi: 10.1016/j.procir.2022.10.013.

[22] A. Morvayova, L. Fabbiano, N. Contuzzi, F. Caiazzo, and G. Casalino, "On the influence of building position on dimensional accuracy and surface quality of aluminum blocks manufactured by L-PBF," *Opt. Laser Technol.*, vol. 167, p. 109830, 2023, doi: 10.1016/j.optlastec.2023.109830.

[23] J. K. Veetil, M. Khorasani, A. Ghasemi, B. Rolfe, I. Vrooijink, K. van Beurden, S. Moes, and I. Gibson, "Build position-based dimensional deviations of laser

powder-bed fusion of stainless steel 316L," *Precis. Eng.*, vol. 67, pp. 58–68, 2021, doi: 10.1016/j.precisioneng.2020.09.024.

[24] R. Mendricky, "Determination of measurement accuracy of optical 3D scanners," *MM Sci. J.*, no. 6, pp. 1565–1572, 2016, doi: 10.17973/MMSJ.2016.

[25] A. Yaghi, S. Ayvar-Soberanis, S. Moturu, R. Bilkhu, and S. Afazov, "Design against distortion for additive manufacturing," *Addit. Manuf.*, vol. 27, pp. 224–235, 2019, doi: 10.1016/j.addma.2019.03.010.

[26] N. Peter, Z. Pitts, S. Thompson, and A. Saharan, "Benchmarking build simulation software for laser powder bed fusion of metals," *Addit. Manuf.*, vol. 36, p. 101531, 2020, doi: 10.1016/j.addma.2020.101531.

[27] S. Giganto, S. Martínez-Pellitero, E. Cuesta, V. M. Meana, and J. Barreiro, "Analysis of Modern Optical Inspection Systems for Parts Manufactured by Selective Laser Melting," *Sensors*, vol. 20, no. 11, p. 3202, 2020, doi: 10.3390/s20113202.

[28] S. Gruber, C. Grunert, M. Riede, E. López, A. Marquardt, F. Brueckner, and C. Leyens, "Comparison of dimensional accuracy and tolerances of powder bed based and nozzle based additive manufacturing processes," *J. Laser Appl.*, vol. 32, no. 3, p. 32016, 2020, doi: 10.2351/7.0000115.

[29] M. Moshiri, S. Candeo, S. Carmignato, S. Mohanty, and G. Tosello, "Benchmarking of Laser Powder Bed Fusion Machines," *JMMP*, vol. 3, no. 4, p. 85, 2019, doi: 10.3390/jmmp3040085.

[30] F. Zongo, A. Tahan, A. Aidibe, and V. Brailovski, "Intra- and Inter-Repeatability of Profile Deviations of an AlSi10Mg Tooling Component Manufactured by Laser Powder Bed Fusion," *JMMP*, vol. 2, no. 3, p. 56, 2018, doi: 10.3390/jmmp2030056.

[31] J. Montero, S. Weber, C. Petroll, S. Brenner, M. Bleckmann, K. Paetzold, and V. Nedeljkovic-Groha, "Geometrical Benchmarking of Laser Powder Bed Fusion Systems Based on Designer Needs," *Proc. Des. Soc.*, vol. 1, pp. 1657–1666, 2021, doi: 10.1017/pds.2021.427.

[32] P. Minetola, M. Galati, F. Calignano, L. Iuliano, G. Rizza, and L. Fontana, "Comparison of dimensional tolerance grades for metal AM processes," *Procedia CIRP*, vol. 88, pp. 399–404, 2020, doi: 10.1016/j.procir.2020.05.069.

[33] M. G. Guerra, L. de Chiffre, F. Lavecchia, and L. M. Galantucci, "Use of Miniature Step Gauges to Assess the Performance of 3D Optical Scanners and to Evaluate the Accuracy of a Novel Additive Manufacture Process," *Sensors*, vol. 20, no. 3, p. 738, 2020, doi: 10.3390/s20030738.

[34] B. R. Barbero and E. S. Ureta, "Comparative study of different digitization techniques and their accuracy," *Comput. Aided Des.*, vol. 43, no. 2, pp. 188–206, 2011, doi: 10.1016/j.cad.2010.11.005.

[35] J. Vagovský, I. Buranský, and A. Görög, "Evaluation of Measuring Capability of the Optical 3D Scanner," *Procedia Eng.*, vol. 100, pp. 1198–1206, 2015, doi: 10.1016/j.proeng.2015.01.484.

[36] S. Feng, S. Chen, A. M. Kamat, R. Zhang, M. Huang, and L. Hu, "Investigation on shape deviation of horizontal interior circular channels fabricated by laser powder bed fusion," *Addit. Manuf.*, vol. 36, p. 101585, 2020, doi: 10.1016/j.addma.2020.101585.

[37] M. Moesen, T. Craeghs, J.-P. Kruth, and J. Schrooten, "Robust beam compensation for laser-based additive manufacturing," *Comput. Aided Des.*, vol. 43, no. 8, pp. 876–888, 2011, doi: 10.1016/j.cad.2011.03.004.

[38] Robert Bosch GmbH, Ed., „Fähigkeit von Mess- und Prüfprozessen," Qualitätsmanagement in der Bosch-Gruppe - Technische Statistik Heft 10, Nov. 2019.

[39] J. Franke, T. Koutecký, and D. Koutný, "Comparison of Sublimation 3D Scanning Sprays in Terms of Their Effect on the Resulting 3D Scan, Thickness, and Sublimation Time," *Materials*, vol. 16, no. 18, p. 6165, 2023, doi: 10.3390/ma16186165.

[40] D. Palousek, M. Omasta, D. Koutny, J. Bednar, T. Koutecky, and F. Dokoupil, "Effect of matte coating on 3D optical measurement accuracy," *Opt. Mater.*, vol. 40, pp. 1–9, 2015, doi: 10.1016/j.optmat.2014.11.020.

[41] *VDI 3405 Part 2.1:2020-08 Additive manufacturing processes - Powder bed fusion of metal with laser beam (PBF-LB/M) - Material data sheet aluminium alloy AlSi10Mg*, Beuth Verlag GmbH, Berlin, Aug. 2020.

[42] B. Klein, *Toleranzdesign im Maschinen- und Fahrzeugbau*, 5th ed. Berlin, Boston: De Gruyter Oldenbourg, 2021.

[43] W.-Y. Jywe, C.-H. Liu, and C.-K. Chen, "The min–max problem for evaluating the form error of a circle," *Measurement*, vol. 26, no. 4, pp. 273–282, 1999, doi: 10.1016/S0263-2241(99)00052-4.